Effects of wave propagation anisotropy on the wave focusing by negative refractive sonic crystal flat lenses

S. Alagoz†

Department of Physics, Inonu University, Center Campus, Turkey

(Received 19 April 2012; revised manuscript received 15 May 2012)

In this study, wave propagation anisotropy in a triangular lattice crystal structure and its associated waveform shaping in a crystal structure are investigated theoretically. A directional variation in wave velocity inside a crystal structure is shown to cause bending wave envelopes. The authors report that a triangular lattice sonic crystal possesses six numbers of a high symmetry direction, which leads to a wave convergence caused by wave velocity anisotropy inside the crystal. However, two of them are utilized mostly in wave focusing by an acoustic flat lens. Based on wave velocity anisotropy, the pseudo ideal imaging effect obtained in the second band of the flat lens is discussed.

Keywords: sonic crystal, wave focusing, flat lens, ideal imaging

PACS: 62.65.+k, 43.20.El, 43.35.Cg **DOI:** 10.1088/1674-1056/21/12/126202

1. Introduction

Researchers are interested in crystal structure because of its amazing wave propagation properties, such as wave focusing,[1−10] negative refraction,[11−15] band gap,[16−18] and wave guiding.[19−21] The scalability feature of crystal also enables the development of applications in a wide range of wave spectra containing electromagnetic waves, elastic waves, and acoustic waves.

The periodical inhomogeneity of the medium leads to the breaking of directional symmetry in terms of the wave propagation features inside the crystal lattice and causes wave propagation anisotropy in certain frequency bands. The wave forming features of crystal are closely related to the wave propagation anisotropy that takes place inside the crystal lattice. A useful outcome of wave propagation anisotropy introduced by a triangular lattice crystal is the convergence of wave beams inside the crystal structure, which is utilized in implementing the metamaterial flat lens.

The phenomenon of wave focalization by sonic crystal (SC) and phononic crystal (PnC) has been researched in many directions. One study was based on refraction in a manner similar to that of the optical lens. Such acoustic lenses were practically developed as convex shaped SCs[1] and their focusing mechanism was described well by the lens-maker's formula.[2] This focalization was obtained mainly in the first frequency band. In this frequency band, the phase velocity inside a crystal structure (v) is isotropic and smaller than the phase velocity (c) of the host material (the air for SC). Hence, in order to enable convergence of a wave beam inside the crystal, a convex SC was designed.[1] Another form of wave focusing was reported for SC exhibiting a negative refraction index.[3−7,22−27] Since, the sonic crystal slab refracts beams with a negative effective refraction index (ERI) in the second band,[11−13] the sonic crystal slab can work as a flat lens within the second frequency band.

Recently, the gradient-index PnC slab was developed to obtain a wave focusing effect; it was shown to allow acoustic focusing over a wide range of working frequencies.[28] The slab is thus suitable for several applications, such as flat acoustic lenses and couplers.[29,30] The refractive index along the direction transverse to the phononic propagation was designated as a hyperbolic secant gradient distribution, which results in a wave velocity gradient through the radial axis inside the crystal. In fact, the gradient-index PnC and negative refractive SC flat lens both benefit from the establishment of appropriate wave propagation anisotropy inside the crystal slab.

This article focuses on a detailed investigation of wave propagation anisotropy introduced by negative refractive SC and its role in determining the wave focusing feature of negative refractive flat lenses. Wave propagation anisotropy in PnC, and its effects

†Corresponding author. E-mail: serkan.alagoz@inonu.edu.tr

© 2012 Chinese Physical Society and IOP Publishing Ltd

on negative refraction and wave focusing were discussed by Yang *et al.*,[9] who revealed that propagation anisotropy leads to very large negative refraction, which can be used to focus a diverging ultrasonic beam into a narrow focal spot. Further discussion about the association of the negative refraction with the phase velocity and group velocity was provided in Refs. [14] and [15]. The super-resolution effect of a triangular lattice flat lens was reported to be possible due to the contribution of the steady state propagative components and the amplified evanescent bound modes to the focal point.[24,25,31] Indeed, these extraordinary wave propagation properties, such as the negative refraction of incident waves, are related to the wave propagation anisotropy resulting from the periodical inhomogeneity of the host material of the crystals according to lattice geometry. Hence, there is still need for a basic understanding of the frequency dependence of wave propagation anisotropy appearing in a crystalline structure. Furthermore, its effects on wave motion inside the crystals should be discussed in detail.

In this paper, the authors demonstrate that a directional variation in the average phase velocity for the wave frequencies within the second band provides relevant directional latencies, which result in a coupled convergence of scattered monochromatic wave envelopes inside SCs as represented in Fig. 1(a). Such a directional phase velocity anisotropy appearing between the symmetry directions of triangular lattices (from ΓK_i and ΓM_i, $i = 1, 2, \ldots, 6$) are used to explain the transformation of a convex wave envelope to concave wave envelope throughout its propagation inside the crystal structure within the second band. The authors report that a triangular lattice contains six wave converging directions; one for each K_i high symmetry direction as illustrated in Fig. 1(d). The relation between this special wave propagation anisotropy of the triangular lattice and the hexagonal form of equifrequency contour (EFC) in the second band is explained in detail. Utilization of the high symmetry direction in wave focusing is discussed for the acoustic flat lenses. Besides, the authors confirm that the superresolution of triangular lattice flat lenses is obtained at the lower boundary of the second band.[20]

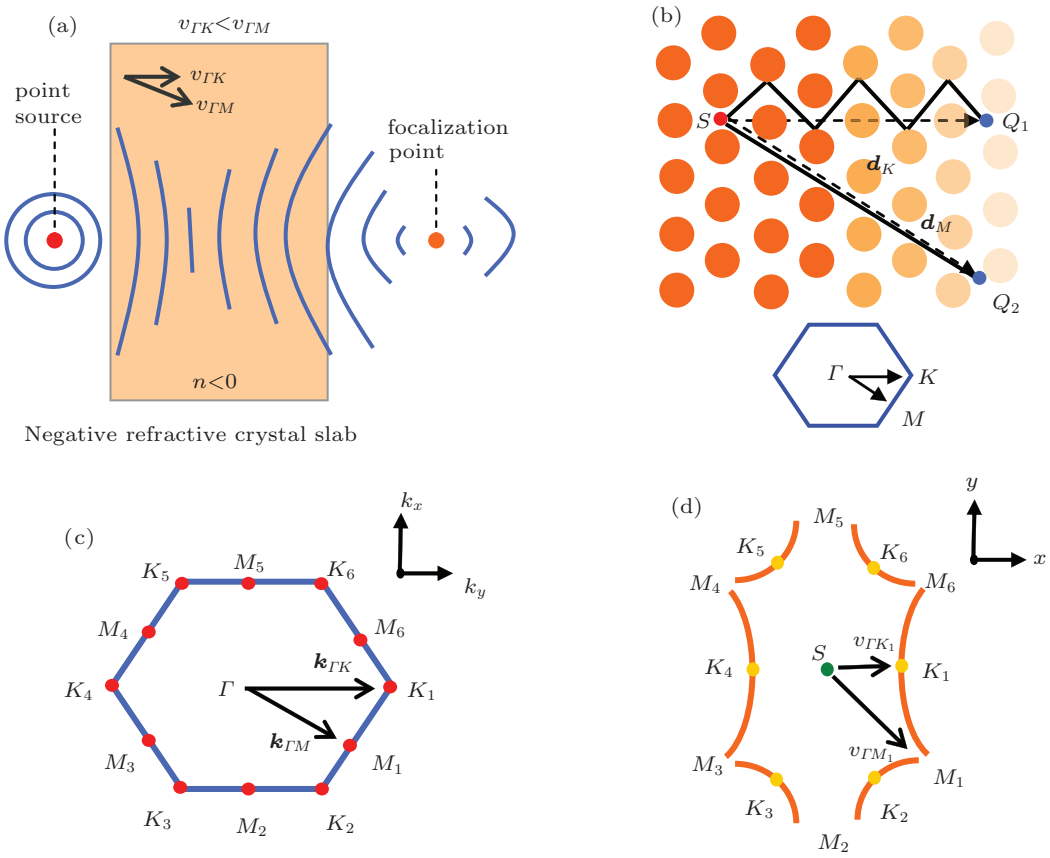


Fig. 1. (colour online) (a) Negative refractive flat sonic lens; (b) wave propagation anisotropy as a result of travelling of wave envelopes around the circular solid scatterers; (c) hexagonal EFC in reciprocal space revealing the wave propagation anisotropy inside a triangular lattice; (d) the resulting wave envelope bending for a point source S placed in the crystal slab in the real space.

The authors used the topographical analyses on equifrequency surface (EFS) of SCs to demonstrate the wave velocity anisotropy inside the sonic crystal structure. These analyses reveal many frequency-dependent directional wave propagation features of crystal structures. The authors observed that the hexagonalization of the EFC motif in the second band is closely related to directional wave propagation anisotropy inside a two-dimensional (2D) triangular lattice. The six K_i high symmetry directions residing on the corner of the hexagonal EFC imply a special propagation anisotropy resulting in bending of scattered wave envelopes in the crystal structure as illustrated in Fig. 1. Finite difference time domain (FDTD) simulation results confirm these six possible wave converging directions that are corresponding to the K_i high symmetry direction in the second band. However, it is observed that only two of them can be effectively used in wave focalization by the negative refractive acoustic flat lenses.

In the detailed analyses of EFC, it is shown that wave velocity anisotropy causing the bending of wave envelopes inside SC increases at the lower bounds of the second band. This also provides an explanation for frequency dependence of the focusing point location of triangular lattice flat lenses.[3,24,26] As the wave frequency decreases in the second band, the focal length of the flat lens decreases due to the increase in bending degree of the wave envelope inside the SC. This also leads to the appearance of superior focusing effects at the lower bound frequencies of the second band. On the other hand, the circular form of EFC in the first band indicates isotropic wave propagation in the triangular lattice SC within the first band. This explains well the need for convex shaped SC to obtain a wave focusing effect at the frequencies in the first band.[1]

Findings of this study are very useful for comprehending the relations between the wave velocity anisotropy inside the crystal structure and the motif of their EFC characteristics. In practice, it will greatly contribute to enhancement of applications utilizing crystal structure such as the flat lenses. In this sense, a brief discussion on the ideal imaging effect of a negative refractive flat lens is presented in the further sections.

The rest of the present paper is organized as follows. The methods used in numerical analyses are briefly introduced in Section 2. The analysis results demonstrating the wave propagation anisotropy contributing wave focalization via triangular lattice sonic crystal flat lenses are presented in Section 3. In Section 4, a short discussion on the ideal imaging effect is given in the light of the analysis presented in Section 2.

2. Numerical methods

In this section a brief introduction of the numerical method used to analyse a test SC is presented. The SC used in test is an equilateral triangle lattice SC made of a circular aluminium scatterer rod in the air. The lattice constant is 30 mm and the radius of the aluminium scatterer rod is 10 mm. Density of the aluminium rod and the air are taken to be 2.7 g/cm^3 and 1.4 g/cm^3, respectively. Filling ratio of the SC is 0.40. Speed of sound (c) is taken to be 340 m/s in calculation.

Throughout this paper, the term directional wave velocity refers to the norm of phase velocity vector in the direction of wave vector $\boldsymbol{k}$, and can be mathematically expressed as $|\boldsymbol{v}| = w/|\boldsymbol{k}|$. The term of monochromatic wave velocity also refers to the phase velocity.

2.1. Plane wave expansion method

EFS is the preferable characteristic for the dispersion analysis of the crystal structure in the reciprocal space. EFC characteristic of the crystal structure provides useful information about the frequency-dependent wave propagation feature of the crystal structure. The plane wave expansion (PWE) method[19,32,33] has been widely used to obtain the equifrequency contour (EFC) and band structure (BS) to indicate the frequency ranges of negative refraction and band gaps.

In the PWE method, the Floquet–Bloch theorem is applied to the wave equation given by Eq. (1) and then the eigenvalue equation obtained is solved for an adequate number of plane waves.[19] Finally, $w_n(k)$ eigenvalues can be obtained for frequency bands ($n = 1, 2, 3, \ldots$) to draw band structures and the EFC characteristics.

$$\nabla \cdot (\rho \cdot \nabla p) - \frac{1}{K} \cdot \frac{\partial^2 p}{\partial u^2} = 0. \tag{1}$$

Here, p is the pressure, $\rho = \rho_{\mathrm{h}}/\rho_{\mathrm{s}}$ is the normalized medium density, and $K = K_{\mathrm{s}}/K_{\mathrm{h}}$ is the normalized bulk modulus. The parameters ρ_{h} and ρ_{s} are the density of the host material and the density of the scatterer material, respectively. The parameters K_{h} and K_{s} are the bulk modulus of the host material and

the bulk modulus of the scatterer material, respectively. The u parameter is the normalized time and expressed as $u = c_0 \cdot t$, where c_0 is the speed of sound in the host material. EFS analysis of the SC presented in this paper are calculated by using the PWE method with 441 plane waves.

2.2. FDTD-based acoustic wave propagation simulation

The FDTD-based acoustic wave simulations are widely employed in spatiotemporal analysis of SC.[3,19,24] In this paper, the FDTD simulation results of 2D triangular lattice test SC are used for confirming EFC analyses results.

In the FDTD simulation, the linear acoustic wave equations, given by Eq. (2), are numerically solved by applying both temporal and spatial derivatives to the central symmetric finite difference approximation.[19] Then the obtained finite difference equations are calculated for a sampled solution point grid of the spatial domain with a fine time increment.

$$\frac{\partial v}{\partial u} = -\underline{\rho}.\nabla p \quad \text{and} \quad \frac{\partial p}{\partial u} = -\overline{K} \cdot \nabla \cdot \boldsymbol{v}. \tag{2}$$

Here, $\boldsymbol{v}$ denotes the normalized particle velocity, and p represents the pressure. In the simulation, the time increment (Δt) is set to be 1 μs and this provides roughly 125-point resolution for a period of simulated acoustic wave in the time domain. The spatial increments (Δx, Δy)are configured to 1 mm for a square grid of the sampled solution point, which provides roughly 40-point spatial resolution for a wavelength of the simulated acoustic wave.

3. Analysis of monochromatic wave propagation anisotropy in triangular lattice sonic crystal

When the wavelength of the incident wave is approximate to half of the lattice constant, which particularly coincides with the second band of the triangular lattice SC ($0.6 < a/\lambda$), the acoustic wave begins to scatter and travel inside an SC structure. In this case, similar to the well-known electromagnetic waveguide of the rectangular cross section ($\lambda < 2a$), the scattered wave envelopes travel around the solid scatterers inside the SC because of the high reflective index of the scattering material, which is comprised of solid rods in a circular cross-section in the air. These motions of wave envelopes around the periodic scatterer arrays result in a directional variation in the path lengths for the equal distances inside the crystal structure (See Fig. 1(b)). This leads to a difference in directional phase delay among the scattered wave envelopes travelling in the SC and thus introduces a directional difference of the average phase velocity, namely a wave propagation anisotropy, inside the SC. These differences in directional path length depend strongly on the crystal lattice geometry, the parameters of the lattice (a, r), and the wavelength of the wave. Accordingly, a wave velocity anisotropy that is caused by the directional path length difference behaves as the hexagonalization of the second band EFS surface ($0.6 < a/\lambda < 1$) in the first Brillouin zone (BZ) of the triangular lattice.

A triangular lattice SC establishes a six-fold high symmetry direction in a hexagon formed in the first BZ as illustrated in Fig. 1(c). An investigation of directional phase velocity between ΓK and ΓM is sufficient to demonstrate the bending character of the wave envelope in the real space as demonstrated in Fig. 1(d). Therefore, we numerically calculate the rate of the phase velocity in the direction of ΓK ($v_{\Gamma K}$) to the phase velocity in the direction of ΓM ($v_{\Gamma M}$) for a wave frequency of w by means of the EFC, expressed as

$$\frac{v_{\Gamma K}}{v_{\Gamma M}} = \frac{|\boldsymbol{k}_{\Gamma M}(w)|}{|\boldsymbol{k}_{\Gamma K}(w)|}, \tag{3}$$

where $\boldsymbol{k}_{\Gamma K}(w)$ and $\boldsymbol{k}_{\Gamma M}(w)$ are wave vectors extending from Γ point to EFC with a frequency of w in the direction of ΓK and the direction of ΓM, respectively. Figure 2 illustrates EFC plots and associated phase velocity distribution in Figs. 2(a) and 2(b) for the second band and in Figs. 2(c) and 2(d) for the first band. As demonstrated in Fig. 2(b), $v_{\Gamma K}$ is the lowest monochromatic average wave velocity and $v_{\Gamma M}$ is the highest monochromatic average wave velocity in the second band due to the hexagonal motif of EFC in Fig. 2(a). The $v_{\Gamma K}/v_{\Gamma M}$ rate indicates the degree of the bending of the coupled wave envelopes propagating towards the directions between ΓK–ΓM.

Figure 3(a) demonstrates the directional wave velocity anisotropies calculated for some values of normalized frequency (a/λ) in the second band. The phase velocity of wave propagating in the direction with θ angle in the SC is inversely proportional to the length of the wave vector in this direction ($v_{\Gamma\theta}(w) = |\boldsymbol{k}_{\Gamma\theta}(w)|^{-1} w$). Thus, the EFC characteristics of the crystal structure can reveal the wave propagation features of the lattice in the real space. In an earlier work, the dependence of the phase velocity on the angle of propagation direction (θ) was reported and utilized in the controlling phase via a phononic crystal slab.[31]

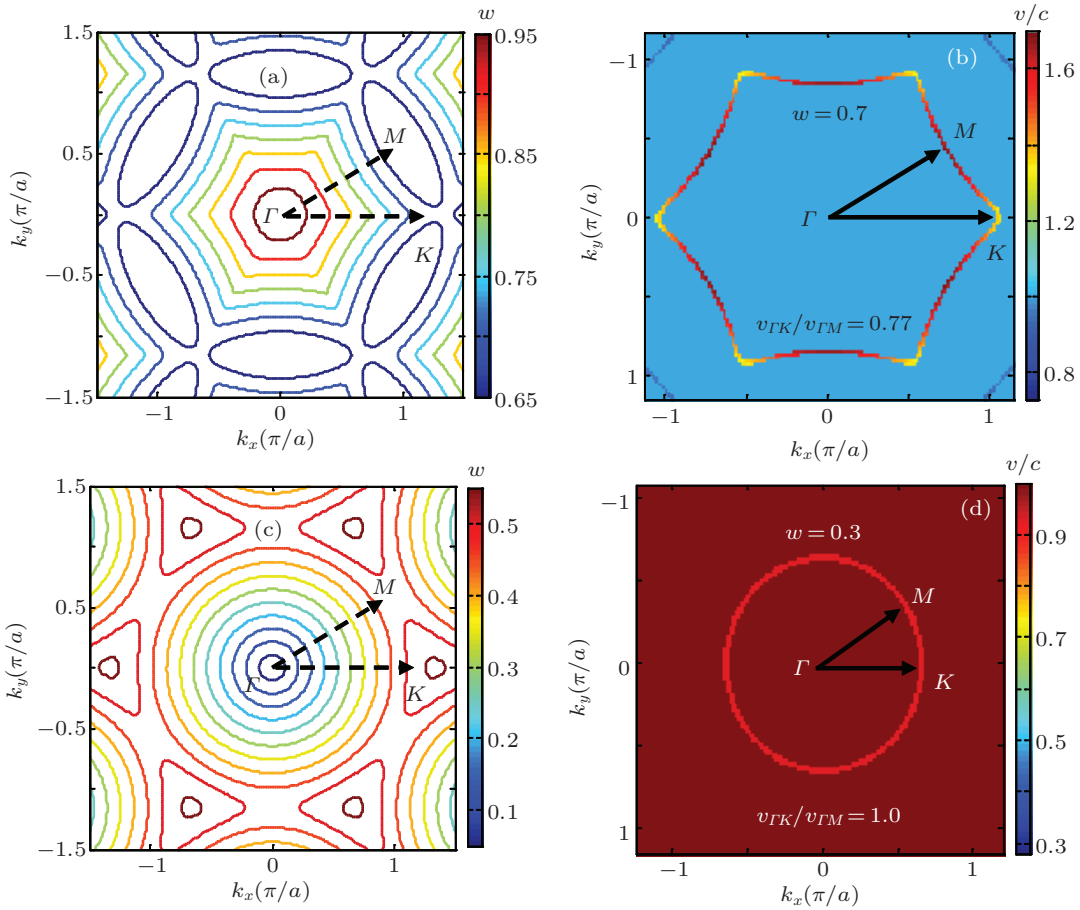


Fig. 2. (colour online) EFC ((a) and (c)) and associated phase velocity distribution examples ((b) and (d)) for an equilateral triangle lattice SC with the lattice parameters of $a = 0.030$ m, $r = 0.010$ m; a directional anisotropy in monochromatic wave velocity (b) as a result of hexagonal EFC at the normalized frequency of 0.7 in the second band; an isotropic wave velocity (d) as a result of circular EFC at the normalized frequency of 0.3 in the first band.

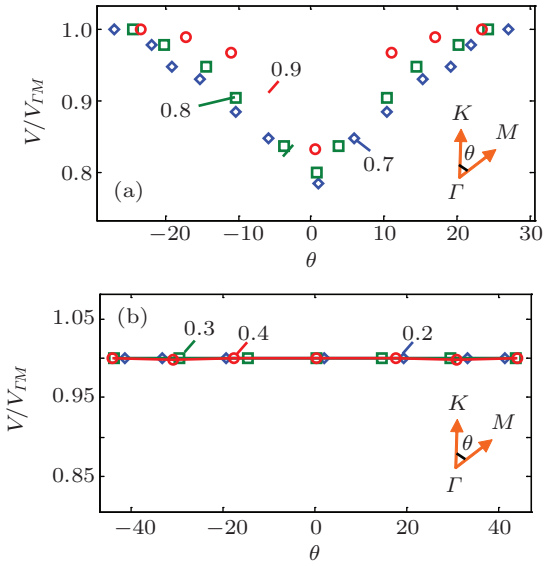


Fig. 3. (colour online) (a) Ratios of the phase velocity (in the direction of θ angle) to v_{pK} at the normalised frequencies of 0.7, 0.8, and 0.9 in the second band; (b) ratios of phase velocity (in the direction of θ angle) to v_{pM} at the normalised frequencies of 0.3, 0.4, and 0.5 within the first band.

Figures 2(d) and 3(b) demonstrate that an isotropic wave propagation occurs in the first band, owing to the circular shape of EFC. The main reason is that the wave velocity is independent of the direction, and consequently the wave propagates as if it is in a homogenous medium, but with a lower wave velocity. This effect appears largely when the wavelength is greater than the approximate length of two lattice constants, $a/\lambda < 0.6$, which coincides with a frequency range in the first band. Thus, the waveform shaping for the wave focusing in the first band is achieved by giving the crystal structure a convex form.[1]

In a 2D crystal structure, the group velocity in a frequency band is expressed as

$$\boldsymbol{V}_{\mathrm{g}} = \left(\frac{\partial w_m}{\partial k_x}, \frac{\partial w_m}{\partial k_y} \right),$$

where $m = 1, 2, 3, \ldots$ denotes the band number. The opposition of group velocity vector to incident wave vector ($\boldsymbol{k}$) originating from Γ indicates the existence of a backward wave and a negative refraction index.[12,14] The direction of the group velocity vector was largely used to reveal the type of refraction [11−13,15] (negative or positive) and the self-collimating effect.[15,20,21]

The group velocity vectors presented across the EFC of the second band shown in Fig. 4(a) also indicate the existence of anisotropic wave propagation property in the second frequency band. Hexagonalization of the second band EFC causes the direction of the group velocity vector to turn towards the direction of ΓK_i. The pointing of the group velocity vector towards ΓK_i as represented in Fig. 4(b) implies the bending of the backward wave envelopes towards the direction of ΓK_i inside the SC. Thus, each ΓK_i direction in the first BZ forms a focal axis in real space for the triangular lattice flat lenses. In the first band, the divergence of forward wave envelopes is evident so that the group velocity vector and the wave vector are in the same directions as shown in Figs. 4(c) and 4(d).

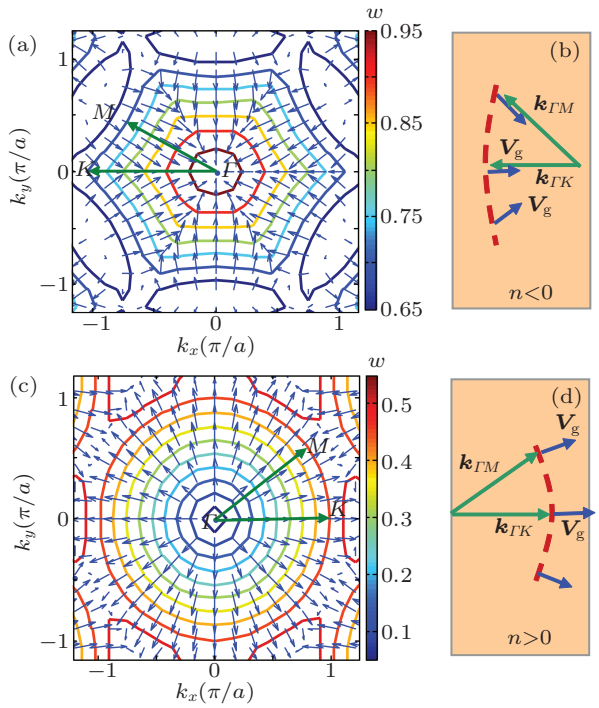


Fig. 4. (colour online) Group velocity vectors ($\boldsymbol{V}_g$'s) associated with EFC for the second band (a) and for the first band (c). Illustrations for a converging backward wave front inside the SC in the second band (b) and a diverging forward wave front in the first band (d).

Figure 5(a) demonstrates the frequency dependence of $v_{\Gamma K}/v_{\Gamma M}$ rate in the second band. At the bottom frequency of the second band, $v_{\Gamma K}/v_{\Gamma M}$ rate takes its smallest value and indicates a maximum anisotropy in wave propagation between the directions of ΓK and ΓM. As frequency increases, the ratio of $v_{\Gamma K}/v_{\Gamma M}$ increases and the degree of wave bending capability inside the SCs decreases accordingly. Simulation results in Fig. 7 confirm this effect. This effect explains well the previous observations that the focal point of the SC moves away from the crystal surface as the frequency increases.[24,26]

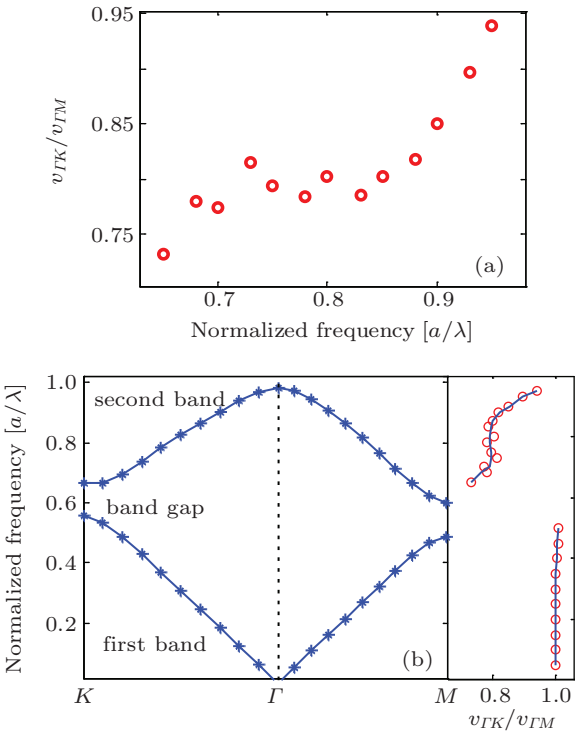


Fig. 5. (colour online) The v_{pK}/v_{pM} ratio (circle) and its interpolated curvature (solid line) versus the normalized frequency (a), and the band structures and v_{pK}/v_{pM} ratio for the first and second band (b). In a range of 0.66–0.92 in the second band, a flat SC bends wave envelopes because of the anisotropy in wave velocity ($v_{pK}/v_{pM} < 1$).

Figure 5(b) illustrates the band structure plots, which are attached to the $v_{\Gamma K}/v_{\Gamma M}$ ratio calculated for the first and second band. In the first frequency band as discussed previously, the SC does not exhibit a proper phase velocity variation due to the circular shape of the EFC. A band gap above the first band severely attenuates wave transmission up to the second band. A significant wave velocity anisotropy between the directions of ΓK and ΓM is shown by the SC at the lower bound of the second band, and this

indicates a strong wave bending degree at the lower bound of the second band. This observation supports a recent explanation given for crystal superlenses:[24] super-resolution can be favourably achieved in the bound mode of the crystal slab with a nearly flat dispersion curve, which appears in the lower frequency region of the band.

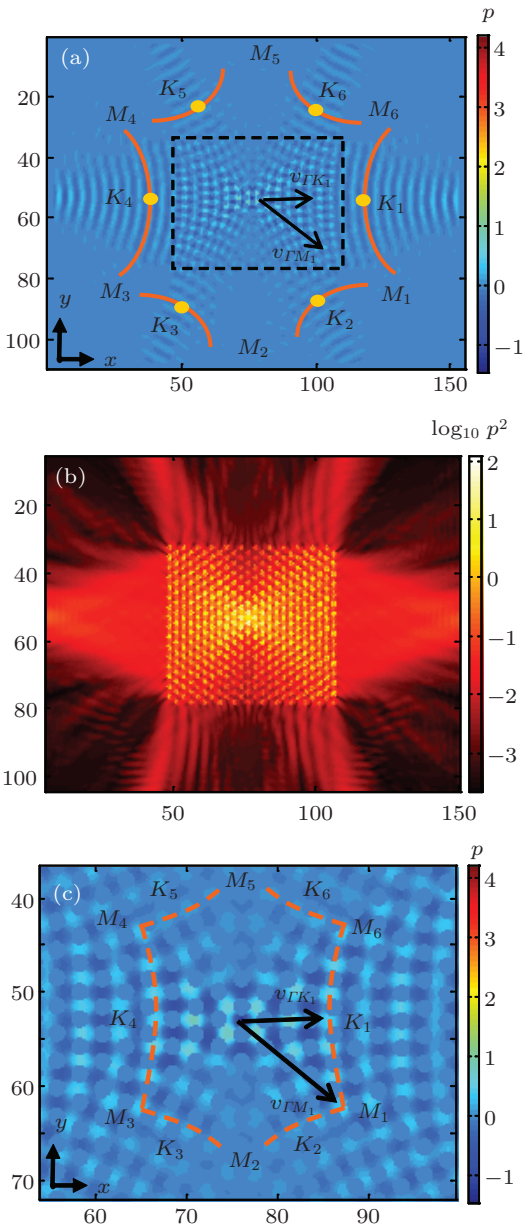


Fig. 6. (colour online) Pressure field patterns ((a) and (c)) and the pressure field intensity distribution with $\log_{10}$ scaling (b) for a point source at $f = 7950$ Hz (0.7 normalized frequency) placed in the centre of the triangular lattice crystal slab with $a = 0.030$ mm and $r = 0.010$ mm. Hexagonal evolution of wave propagation in the SC confirms that the average phase velocity anisotropy leads to focusing.

In order to confirm these findings, FDTD simulations are conducted for the test SC. For this purpose, a point source working at 7950 Hz (the normalised frequency of 0.7) is placed inside the crystal structure. The aim of the embedded point source configuration inside the crystal structure is to get rid of possible effects associated with classical geometric acoustics, such as negative refraction of beams at the interface. This allows us to observe the wave propagation anisotropy originating only from the structural factors of the crystal. The pressure field patterns and the pressure field intensity distribution shown in Fig. 6 clearly demonstrate the wave bending effect resulting from wave velocity anisotropy introduced by the triangular lattice SC, which fully supports the results of EFC analyses of the SC. In the directions of ΓM_1–ΓK_1–ΓM_6 and ΓM_3–ΓK_3–ΓM_4, two major concave bendings of the wave envelope are apparent in the simulation results. This major concave bending actually leads to wave focussing along the x axis on a point source placed nearby a flat SC lens. In the directions of ΓM_4–ΓK_5–ΓM_5, ΓM_5–ΓK_6–ΓM_6, ΓM_1–ΓK_2–ΓM_2, and ΓM_3–ΓK_3–ΓM_2, four minor concave bendings of wave envelopes appear on both sides of the two major concave bendings in Fig. 6(a). In practice, they do not efficiently contribute to focussing points of flat SC lenses, because the angles of beams in these directions are generally greater than the critical angle of Snell's Law.

It should be noted that a triangular-lattice flat SC can effectively focus the wave beams in the direction between ΓM_1–ΓK_1–ΓM_6 and ΓM_3–ΓK_3–ΓM_4 where major concave bending takes place. Figure 7 demonstrates the frequency dependences of major wave envelope bending throughout ΓM_1–ΓK_1–ΓM_6. As wave frequency increases, $v_{\Gamma K}/v_{\Gamma M}$ ratio increases as suggested in Fig. 5(a). The influence of the increase in $v_{\Gamma K}/v_{\Gamma M}$ ratio depends on wave frequency as clearly observed in Fig. 7. As frequency increases from 0.7 to 0.9, the wave envelopes exhibit less bending of wave envelopes inside the crystal because of the increase in ratio $v_{\Gamma K}/v_{\Gamma M}$.

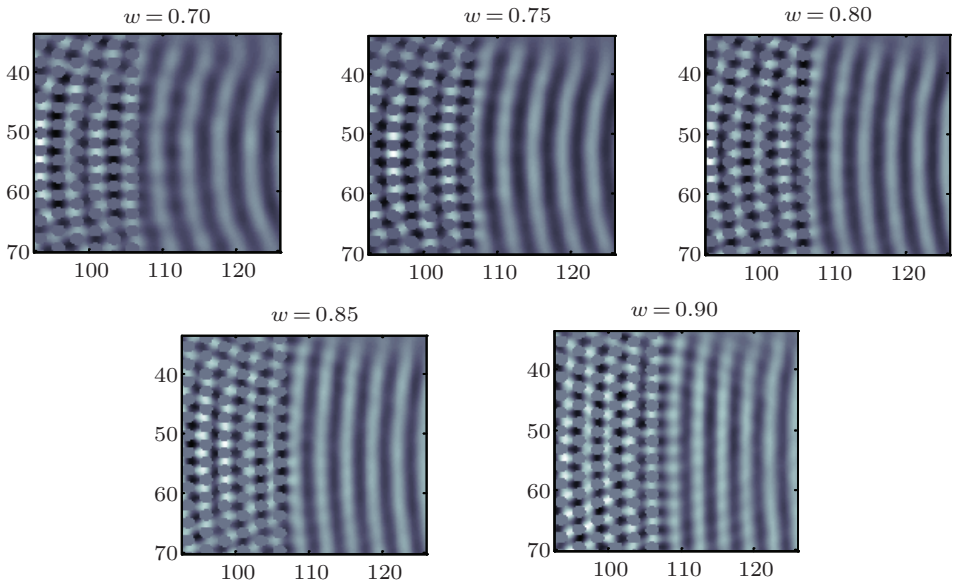


Fig. 7. (colour online) FDTD simulation pressure field patterns in the vicinity of crystal interface for some different normalized frequencies of a point source placed in the centre of the triangular lattice crystal slab shown in Fig. 6. The ratio of v_{pK}/v_{pM} calculated from the EFC of the second band is 0.77 (0.79, 0.80, 0.80, 0.85) for a normalized frequency of 0.70 (0.75, 0.80, 0.85, 0.90) respectively.

4. Discussion on the ideal imaging effect of triangular lattice sonic crystal flat lenses

The ideal imaging of a flat lens is based on ray-trace analysis. What is considered here is the focusing effect that emerges when all rays coming from a point source are refracted with an ERI of -1 ($n = -1$).[7,8,15] This theoretically allows the convergence of all refracted beams into a single focal point. Thus, the ideal imaging not only provides a very intensive wave focalization effect compared with the case of $n \neq -1$, but also forms, theoretically, a perfect image of a point source.

In order to derive the $v_{\Gamma K}/v_{\Gamma M}$ condition conforming to the theoretical ideal imaging, an analytical treatment based on beam intersections with a phase coupling of converging beams is performed regarding the ray-trace analysis shown in Fig. 8(a). This figure presents a geometrical interpretation of the theoretical ideal imaging. More specifically, the phase coupling of converging wave envelopes infers an equal travelling time (T) of the scattered wave envelopes to the focusing point for all values of refracted beam angle (θ). By using the geometrical analysis presented in Fig. 8(a) and considering the formulation $d = s + f$, which is valid in the case of $n = -1$,[8,24] the following expression that describes the required wave velocity anisotropy condition for ideal imaging by a negative refractive flat lens is obtained

$$\frac{v_{\Gamma K}}{v_{\Gamma\theta}} = \frac{d - \dfrac{v_{\Gamma K}}{c}(L_1 + L_2 - d)}{L_1 + L_2}. \tag{4}$$

Then considering that $v_{\Gamma K}/c \cong 1$, the wave velocity inside the SC must be equal to the wave velocity in the air (c) in the case of $n = -1$, and equation (4) can be simplified into

$$\frac{v_{\Gamma K}}{v_{\Gamma\theta}} \cong 2\cos\theta - 1. \tag{5}$$

The dependence of the refraction index of the SC on beam angle θ can be expressed as $n = c/v_{\Gamma\theta} = -c\,|\boldsymbol{k}_{\Gamma\theta}|/w$ in monochromatic wave propagation inside the crystal.[8,26] Therefore, a triangular lattice crystal has a hexagonal equifrequency contour in the second band; the negative refraction index varies due to variation in $|\boldsymbol{k}_{\Gamma\theta}|$ as illustrated in Fig. 8(b). In Refs. [8] and [26], a circular approximation to a hexagonal equifrequency contour was used to express the effective refraction index (ERI) of SC. A triangular lattice SC does not inherently exhibit the theoretical ideal imaging, which requires all of the refracted beams to each have an index of -1, in

the second band. The main reason is that the hexagonal shape of the equifrequency contour in the second band does not overlap perfectly the circular form of the dispersion cone of the air. This indeed makes the refraction index of the flat lens depend on beam angle θ. Thus, it is difficult to observe a theoretical ideal imaging effect at the lower bounds of the second band. Figure 8(b) clearly illustrates mismatches between a hexagonal equifrequency contour of SC (hexagonal anisotropy regarding wave vectors $\boldsymbol{k}_{\Gamma\theta}$) and the circular equifrequency contour of the air. However, a pseudo-ideal imaging effect is possible in the ΓK direction associated with an appropriate bending of wave envelopes, which corresponds to the case of the all refracted beam index being -1 ($n = -1$).

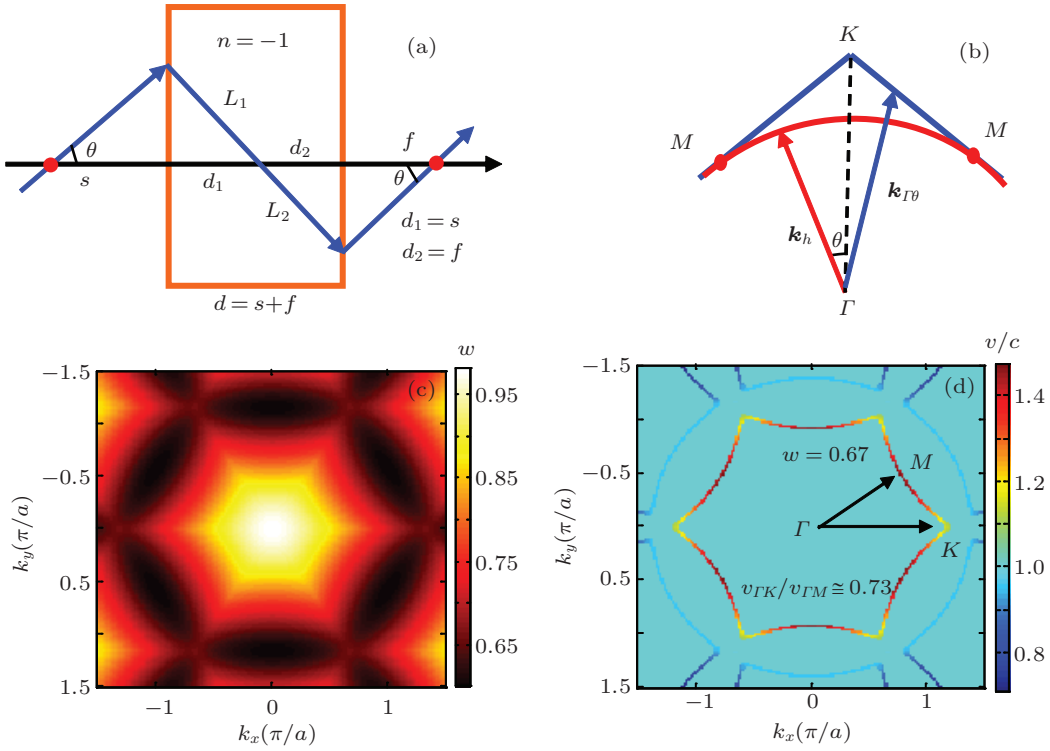


Fig. 8. (colour online) (a) Ray-trace analysis for ideal imaging; (b) hexagonal EFC of a triangular lattice in the second band in blue and circular EFC of the air in red; (c) EFS of the SC used in the test and circular EFC of the air at a normalized frequency of 0.67 (dashed white line); (d) phase velocity distribution at a normalized frequency of 0.67.

The angle between ΓM and ΓK is 30° in an equilateral triangle lattice. The required $v_{\Gamma K}/v_{\Gamma M}$ ratio leads to a pseudo ideal imaging effect, which is calculated to be roughly 0.73 by Eq. (5) for $\theta = 30°$. According to the $v_{\Gamma K}/v_{\Gamma M}$ analysis on the second band EFS shown in Fig. 8(c), the ratio of $v_{\Gamma K}/v_{\Gamma M} \cong 0.73$ is possible roughly at the normalized frequency of 0.67 for the test SC.

Figure 9 illustrates the FDTD simulation results of the imaging effect via pressure field patterns and the logarithmic scaled maximum pressure field intensity distribution. A pseudo-ideal imaging effect conforming to $v_{\Gamma K}/v_{\Gamma M} \cong 0.73$ at a normalized frequency of 0.67 is demonstrated in Fig. 9(a). For comparison, the focusing effect obtained for $v_{\Gamma K}/v_{\Gamma M} \cong 0.80$ at a normalized frequency of 0.75 is also demonstrated in Fig. 9(b). As frequency increases in the second band, the EFC of the crystal turns into an approximately circular form and all angle negative refraction (AANR) becomes dominant in focusing. However, wave-bending capability is somewhat deteriorated. Consequently, pseudo-ideal imaging is possible at $v_{\Gamma K}/v_{\Gamma M} \cong 0.73$ in the lower bound of the second band because negative refracted components in addition to resonantly amplified evanescent components of the SC[24,31,34] can converge to the same focalization region via the appropriate bending of wave envelopes.

The distributions of pressure field intensity over the focal axis for some different frequencies in the second band are presented in Fig. 10, which confirms the pseudo ideal imaging by SC at the normalized frequency of 0.67 and exhibits the most intensive wave focalization. As wave frequency increases, the focusing point shifts away because of the increase of ratio $v_{\Gamma K}/v_{\Gamma M}$ as demonstrated in the previous section.

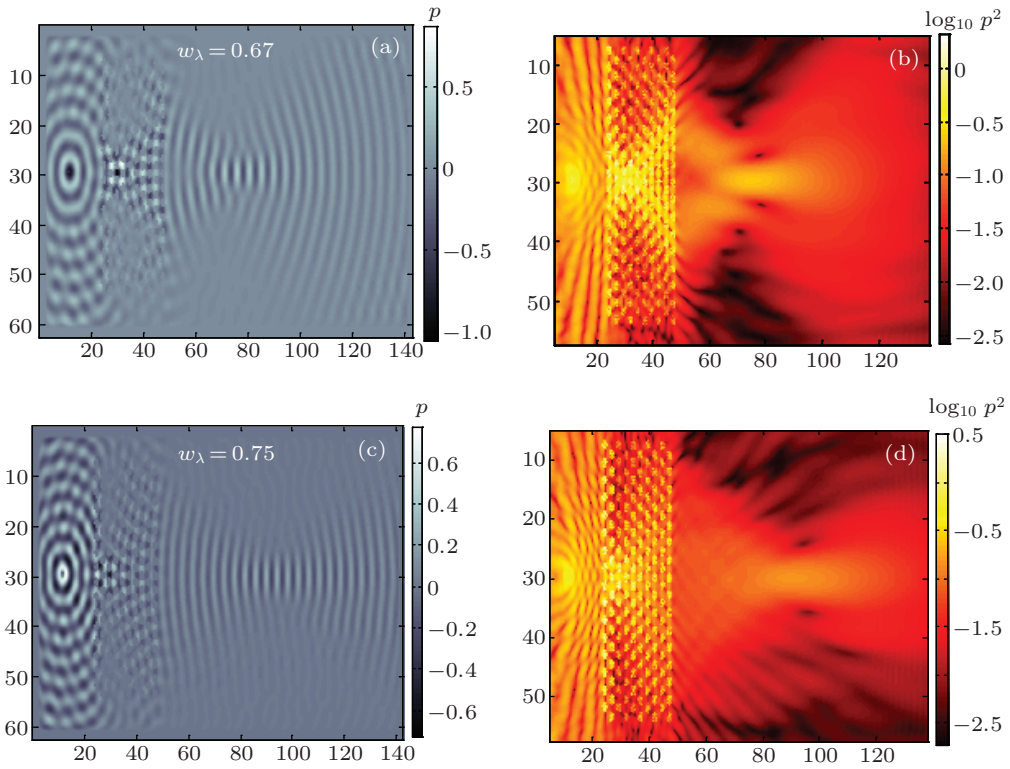


Fig. 9. (colour online) Pressure field patterns ((a) and (c)) and logarithmic scaled pressure field intensity distributions ((c) and (d)), demonstrating the imagings of a point source with a flat SC lens for the normalized frequencies of 0.67 and 0.75.

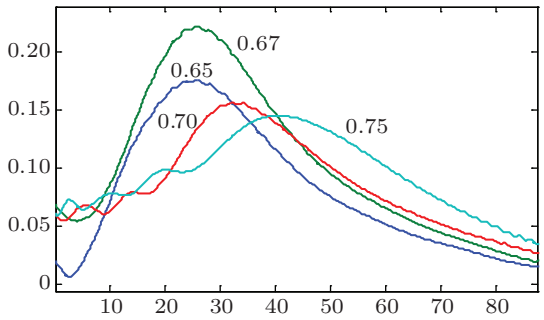


Fig. 10. (colour online) Pressure field intensity distributions over the focal axis for some different frequencies.

5. Conclusions

The directional asymmetry resulting from the solid scatterer placements in the crystal lattice leads to a directional variation in average phase velocity inside an SC and induces frequency-dependent wave propagation anisotropy. This effect appears in a triangular lattice SC when the scattered wave envelopes effectively travel around the scatterers and it causes directional phase delays inside the SC. When this effect appears in the second band, it governs the convergence of scattered wave envelopes inside the SC and plays a role in the wave focusing effect of a negative refractive flat lens. Phase velocity and group velocity analysis regarding the motif of the EFC reveals the features of the anisotropic wave propagation resulting in a wavefront shaping effect inside the SC.

The hexagonal shape of the EFC in the second band reveals a six-fold wave envelope bending direction for each ΓK_i high symmetry direction. Bendings in the directions of ΓM_1–ΓK_1–ΓM_6 and ΓM_3–ΓK_3–ΓM_4 are utilized in the implementation of the perfect flat lenses. The other bending directions exist in ΓM_4–ΓK_5–ΓM_5, ΓM_5–ΓK_6–ΓM_6, ΓM_1–ΓK_2–ΓM_2, and ΓM_3–ΓK_3–ΓM_2. However, they are not effectively utilized in focussing waves coming from a point source placed outside a flat sonic lens. They can be easily observed in the case of an embedded point source configuration inside SC.

Hexagonalization of the EFC increases as the frequency decreases to the lower bound of the second band, implying that the wave velocity anisotropy resulting in bending of the scattered wave envelopes would be more effective at the lower bound of the second band.

It is possible to obtain a pseudo-ideal imaging effect in the lower bound of the second band where the condition of $v_{pK}/v_{pM} \cong 0.73$ is satisfied. At a fre-

quency of pseudo-ideal imaging, the flat lens produces a focusing effect superior to the rest of the second band.

References

[1] Cervera F, Sanchis L, Sanchez-Perez J V, Martinez-Sala R, Rubio C, Meseguer F, Lopez C, Caballero D and Sanchez-Dehesa J 2001 *Phys. Rev. Lett.* **88** 023902

[2] Chao-Hsien K and Zhen Y 2004 *J. Phys.* D: *Appl. Phys.* **37** 2155

[3] Alagoz S 2011 *Meas. Sci. Technol.* **22** 115105

[4] Fang N, Lee H, Sun C and Zhang X 2005 *Science* **308** 534

[5] Yang W P, Wu L Y and Chen L W 2008 *J. Phys.* D: *Appl. Phys.* **41** 135408

[6] Yang S, Page J H, Liu Z, Cowan M L, Chan C T and Sheng P 2004 *Phys. Rev. Lett.* **93** 02430

[7] Sukhovich A, Li J and Page J H 2008 *Phys. Rev. Lett.* B **77** 014301

[8] Qiu C, Zhang X and Liu Z 2005 *Phys. Rev.* B **71** 054302

[9] Yang S, Page J H, Liu Z, Cowan M L, Chan CT and Sheng P 2004 *Phys. Rev. Lett.* **93** 0243301

[10] Feng Z F, Wang X G, Li Z Y and Zhang D Z 2008 *Chin. Phys.* B **17** 1101

[11] Luo C, Johnson S G, Joannopoulos J D and Pendry J B 2002 *Phys. Rev.* B **65** 201104

[12] Feng L, Liu X P, Chen Y B, Huang Z P, Mao Y W, Chen Y F, Zi J and Zhu Y Y 2005 *Phys. Rev.* B **72** 033108

[13] Feng L, Liu X P, Lu M H, Chen Y B, Chen Y F, Mao Y W, Zi J, Zhu Y Y, Zhu S N and Ming N B 2006 *Phys. Rev. Lett.* **96** 014301

[14] Mackay T G and Lakhtakia A 2009 *Phys. Rev.* B **79** 235121

[15] Veselago V, Braginsky L, Shklover V and Hafner C 2006 *J. Comput. Theor. Nanoscience* **3** 1

[16] Zhao H G, Wen J H, Liu Y Z, Yu D L, Wang G and Wen X S 2008 *Chin. Phys.* B **17** 1305

[17] Cai C, Zhu X F, Chen Q, Yuan Y, Liang B and Cheng J C 2011 *Chin. Phys.* B **20** 116301

[18] Wu L Y and Chen L W 2011 *J. Phys.* D: *Appl. Phys.* **44** 045402

[19] Miyashita T 2005 *Meas. Sci. Technol.* **16** 47

[20] Frandsen L H, Lavrinenko A V, Fage-Pedersen J and Borel P I 2006 *Opt. Express* **14** 9444

[21] Cicek A, Kaya O A and Ulug B 2011 *J. Phys.* D: *Appl. Phys.* **44** 205104

[22] Feng L, Liu X P, Chen Y B, Huang Z P, Mao Y W, Chen Y F, Zi J and Zhu Y Y 2005 *Phys. Rev.* B **72** 033108

[23] Perez-Arjona I, Sanchez-Morcillo V J, Redondo J, Espinosa V and Staliunas K 2007 *Phys. Rev.* B **75** 014304

[24] Robillard J F, Bucay J, Deymier P A, Shelke A, Muralidharan K, Merheb B, Vasseur J O, Sukhovich A and Page J H 2011 *Phys. Rev.* B **83** 224301

[25] Luo C, Johnson S G, Joannopoulos J D and Pendry J B 2003 *Phys. Rev.* B **68** 045115

[26] Alagoz S and Alagoz B B 2009 *Appl. Acoustics* **70** 1400

[27] Moussa R, Foteinopoulou S, Zhang L, Tuttle G, Guven K, Ozbay E and Soukoulis C M 2005 *Phys. Rev.* B **71** 085106

[28] Torrent D and Sánchez-Dehesa 2007 *New J. Phys.* **9** 323

[29] Lin S C S, Huang T J, Sun J H and Wu T T 2009 *Phys. Rev.* B **79** 094302

[30] Wu T T, Chen Y T, Sun J H, Steven Lin S C and Huang T J 2011 *Appl. Phys. Lett.* **98** 171911

[31] He Z, Cai F, Ding Y and Liu Z 2008 *Appl. Phys. Lett.* **93** 233503

[32] Economou E N and Sigalas M M 1993 *Phys. Rev.* B **48** 13434

[33] Sigalas M M 1998 *J. Appl. Phys.* **84** 3026

[34] Swinteck N, Robillard J F, Bringuier S, Bucay J, Muralidharan K, Vasseur J O, Runge K and Deymier P A 2011 *Appl. Phys. Lett.* **98** 103508